JGR: Solid Earth

Supporting Information for "Paleomagnetism of the southwest Laurentia large igneous province and Cardenas Basalt: pulsed magmatism during rapid late Mesoproterozoic plate motion"

Yiming Zhang[1, *], Nicolas S. Anderson[1], Mike T. Mohr[2], Lyle L. Nelson[3], Francis A. Macdonald[4], Mark D. Schmitz[2], Olivia G. Thurston[5], William R. Guenthner[5], Karl E. Karlstrom[4], Nicholas L. Swanson-Hysell[1]

[1] University of California, Berkeley, CA 94720, USA
[2] Boise State University, Boise, ID 83725, USA
[3] Department of Earth Sciences, Carleton University, Ottawa, ON K1S 0V9, Canada
[4] University of California, Santa Barbara, CA 93106, USA
[5] Department of Geology, University of Illinois at Urbana-Champaign, Urbana, IL 61801, USA
[6] University of New Mexico, Albuquerque, NM 87131, USA
[*] Correspondence to: yimingzhang@berkeley.edu

List of Supporting Information Figures

List of Tables

Table S1. Compilation of paleomagnetic data collected from mafic sills in central Arizona by Harlan (1993) and Donadini et al. (2011). The study of Donadini et al. (2011) revisited some field areas of Harlan (1993) and resampled some diabase sills in the earlier study. However, the determination of individual cooling units was not clear in Donadini et al. (2011). We compiled data from both studies with a focus on distinguishing individual paleomagnetic sites as distinct cooling units based on geographic and paleomagnetic information provided in the original publications. Data rejected by the original authors are not included. Original "site" level data with better Fisher statistics (higher concentration parameter k values) are preferentially used in cases where repeat sampling of the same cooling unit is interpreted to have happened. We interpret site GD12 and GD13 of Harlan (1993) are the same as site OD in Donadini et al. (2011) and thus recalculated mean statistics. dir_dec—declination; dir_inc— inclination; k—kappa concentration parameter of the site mean direction; a_{95}—95% confidence angle of site mean direction; n—number of samples included in each site; N—number of sites used in calculating the mean statistics by polarity; plat/Plat—pole latitude; plon/Plon—pole longitude. The site level pole locations are recalculating using the directions and site location information provided in the original studies.

site	dir_dec	dir_inc	k	a95	n	slon	slat	pole reference	plon	plat	polarity
GD01-02	279.2	57				249.5	33.7	Harlan, 1993	188.7	26.4	N
GD03	285.3	51.4	165	3.6	11	249.5	33.8	Harlan, 1993	180.7	28.8	N
GD04	295.5	56.6	81.9	7.7	7	249.5	33.8	Harlan, 1993	182.9	38.4	N
GD05	283.2	26	108.5	5.8	7	249.5	33.8	Harlan, 1993	163.9	18.4	N
GD06-07	282.8	48.9				249.3	33.5	Harlan, 1993	179.3	25.8	N
GD08	318	61.2	56.1	5.6	13	249.3	33.5	Harlan, 1993	186.8	56.1	N
GD09	299.2	53.8	21.1	11.5	9	249.3	33.5	Harlan, 1993	178.3	40.3	N
GD10	267.5	38.2	421.5	3.3	6	249.3	33.5	Harlan, 1993	178.7	9.7	N
GD17	285.9	17.1	34.5	8.3	10	249.1	33.6	Harlan, 1993	157.7	18	N
GD18-20	339.6	36.3				249.2	33.5	Harlan, 1993	128	67.5	N
GD22	270.1	40.4	120.3	5.1	8	249.5	33.8	Harlan, 1993	178.9	12.7	N
GD24	297.9	58.5	168	4	9	249.5	33.8	Harlan, 1993	184.8	40.8	N
GD29	306.9	66.4	678.5	2	9	249.4	33.6	Harlan, 1993	197.2	48.2	N
GD30	264.1	33.4	157.6	5.4	6	249.4	33.6	Harlan, 1993	177.8	5.3	N
DF	332.6	69.4	145.1	3.5	13	249.3	33.5	Donadini et al., 2011	212.7	62.5	N
DG	266.2	34.4	58.7	8	7	249.4	33.6	Donadini et al., 2011	176.9	7.4	N
DJ	281.9	52.8	325.5	2.9	9	-110.48	33.65	Donadini et al., 2011	182.8	26.7	N
KD	293.8	13.4	142.3	3.3	14	-110.97	33.89	Donadini et al., 2011	151.2	23.5	N
MD	277.2	50.7	110.4	4.2	12	-110.98	33.87	Donadini et al., 2011	182.9	22.2	N
GD12_GD13_OD	280.8	45.7	313.7	7		-110.98	33.81	Harlan, 1993; Donadini et al., 2011	177.6	23	N
GD11	115.3	-69.9	173.7	4.2	8	-110.96	33.75	Harlan, 1993	24.3	-41	R
GD15-27	224.9	-73.7				-110.5	33.8	Harlan, 1993	103.8	-50.9	R
BD	137.6	-74	66.1	8.2	7	-110.61	33.61	Donadini et al., 2011	36.5	-52	R
WD	199.2	-71	92.1	3.1	24	-110.69	33.55	Donadini et al., 2011	95	-64.4	R

	dir_dec	dir_inc	k	a95	N	Plon	Plat	A95
normal polarity mean	287.6	47.4	14.4	8.5	20	177.4	30.6	8.9
reversed polarity mean	167.4	-77	31.8	16.6	4	239.9	57.5	30.6

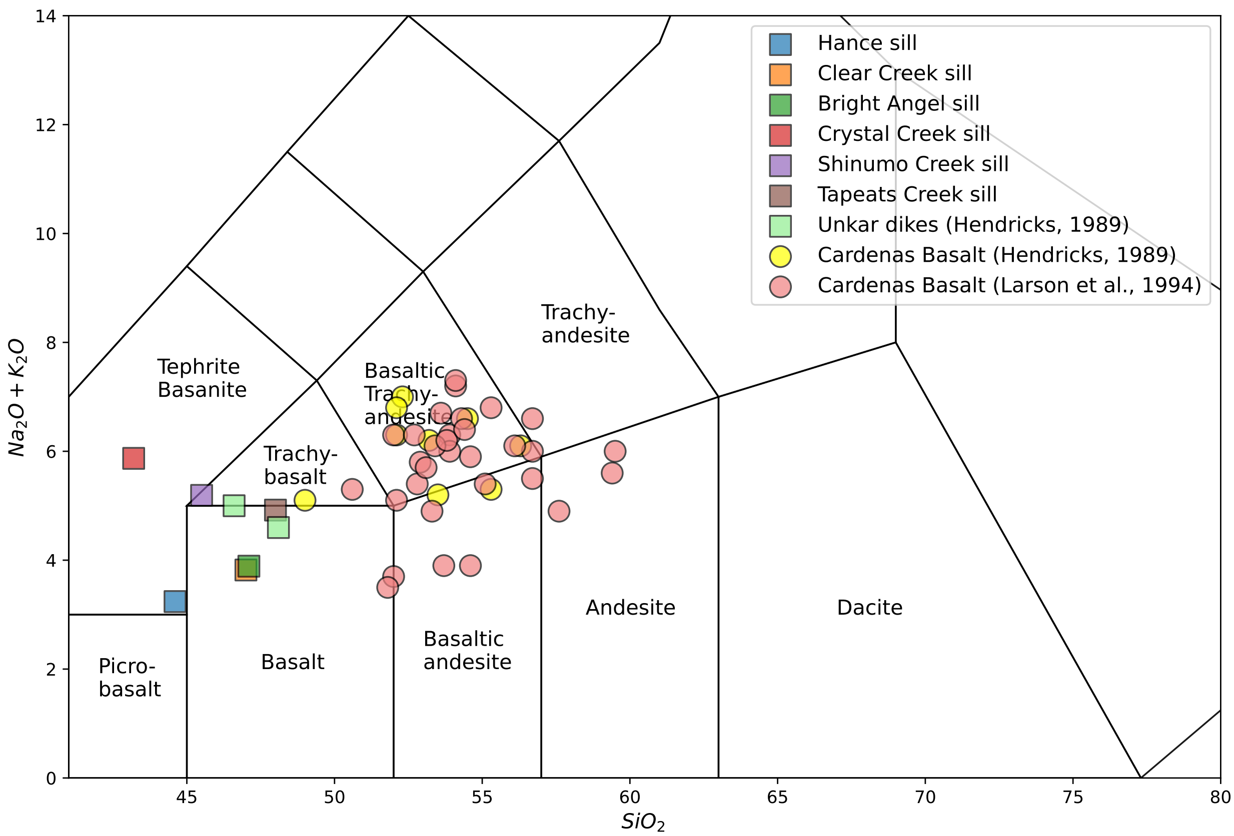

Figure S1. Total alkali-silica diagram of the Cardenas Basalt and mafic intrusions within the Unkar Group. The sills and dikes typically have lower silica content (basalt) than the Cardenas Basalt (basaltic trachy-andesite). Data for the Cardenas Basalt are from Hendricks (1989) and Larson et al. (1994). Data for the intrusions are from Hendricks (1989).

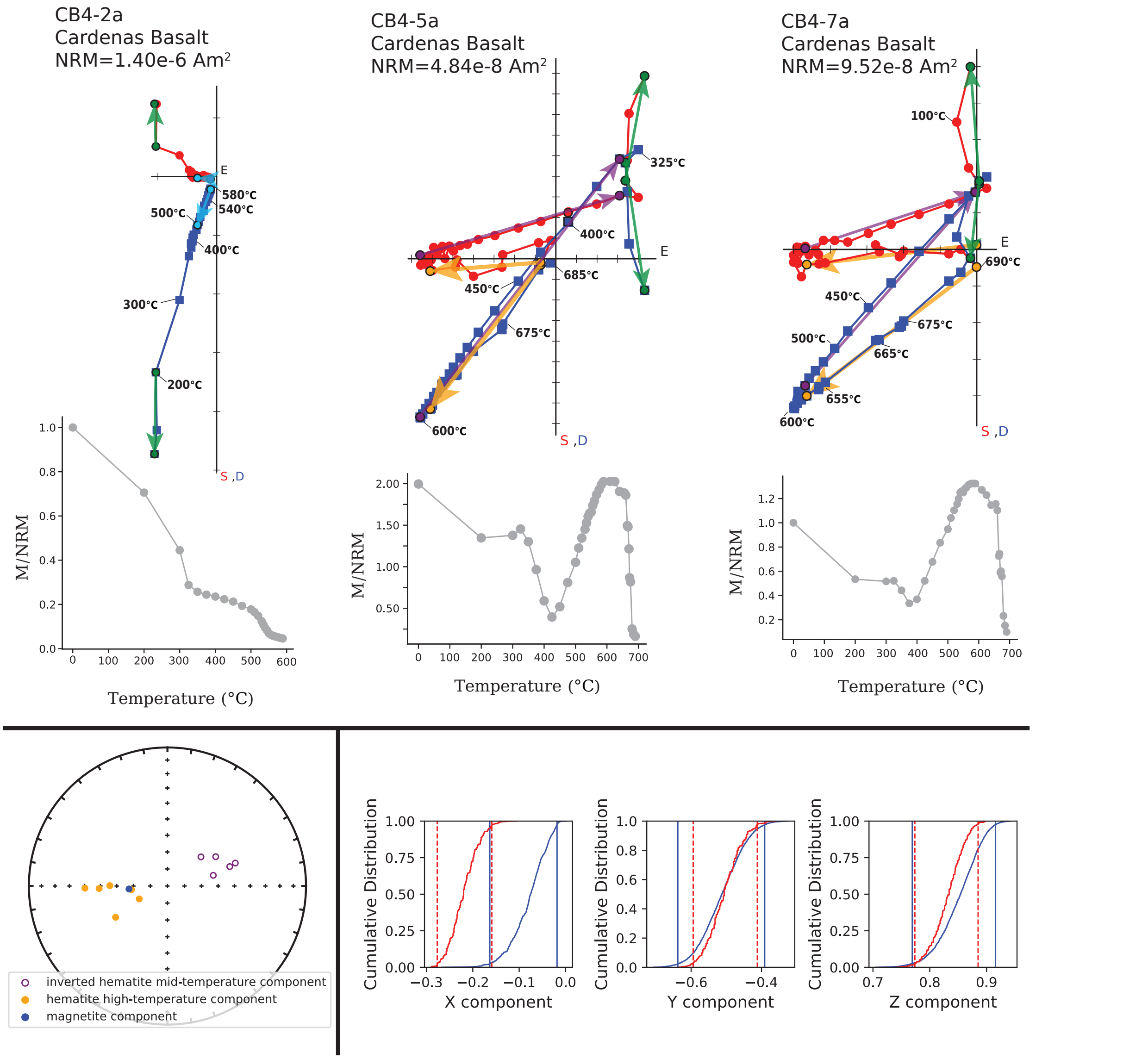

Figure S2. Top panel: Thermal demagnetization data of paleomagnetic specimens collected near the bottom of lava flow CB4. Specimen CB4-2a has a demagnetization behavior similar to other lava flows–after the removal of the present day local field overprint, an origin-trending magnetite-carrying characteristic component unblocks up to 580°C. However, for all other specimens, after the removal of the present day local field overprint by ∼300°C (green vector), their total magnetic moments typically increase as the thermal demagnetization approaches ∼600°C. This mid-temperature component is followed by an origin-trending decay approaching the Nèel temperature of hematite. Bottom panel: Bootstrap reversal test (Tauxe et al., 1991) of the mid-temperature and high-temperature remanence component of CB4. The directions pass the bootstrap reversal test and McFadden and McElhinny (1990) reversal test of with a 'C' classification. The high-temperature component that unblocks sharply near the hematite Nèel temperature has the same polarity with titanomagnetite carried directions in other Cardenas Basalt flows. This similarity is consistent with the hematite forming from oxidation soon after eruption (Haggerty and Baker, 1967). A likely origin of the antipodal component is that it is a self-reversed chemical remanent magnetization held by fine-grained hematite that formed as a result of inversion of maghemite precursors (Hedley, 1968; McClelland, 1987; Mcclelland and Goss, 1993; Swanson-Hysell et al., 2011). This self-reversal behavior is more likely than one that involves the reversal of the geomagnetic field after the emplacement of the CB4 lava flow. No reversed direction is observed in the adjacent lava flows and previous compilations of paleomagnetic data during this time suggest that the Cardenas lava flows were emplaced during a normal-polarity superchron (Swanson-Hysell et al., 2019; Driscoll and Evans, 2016).

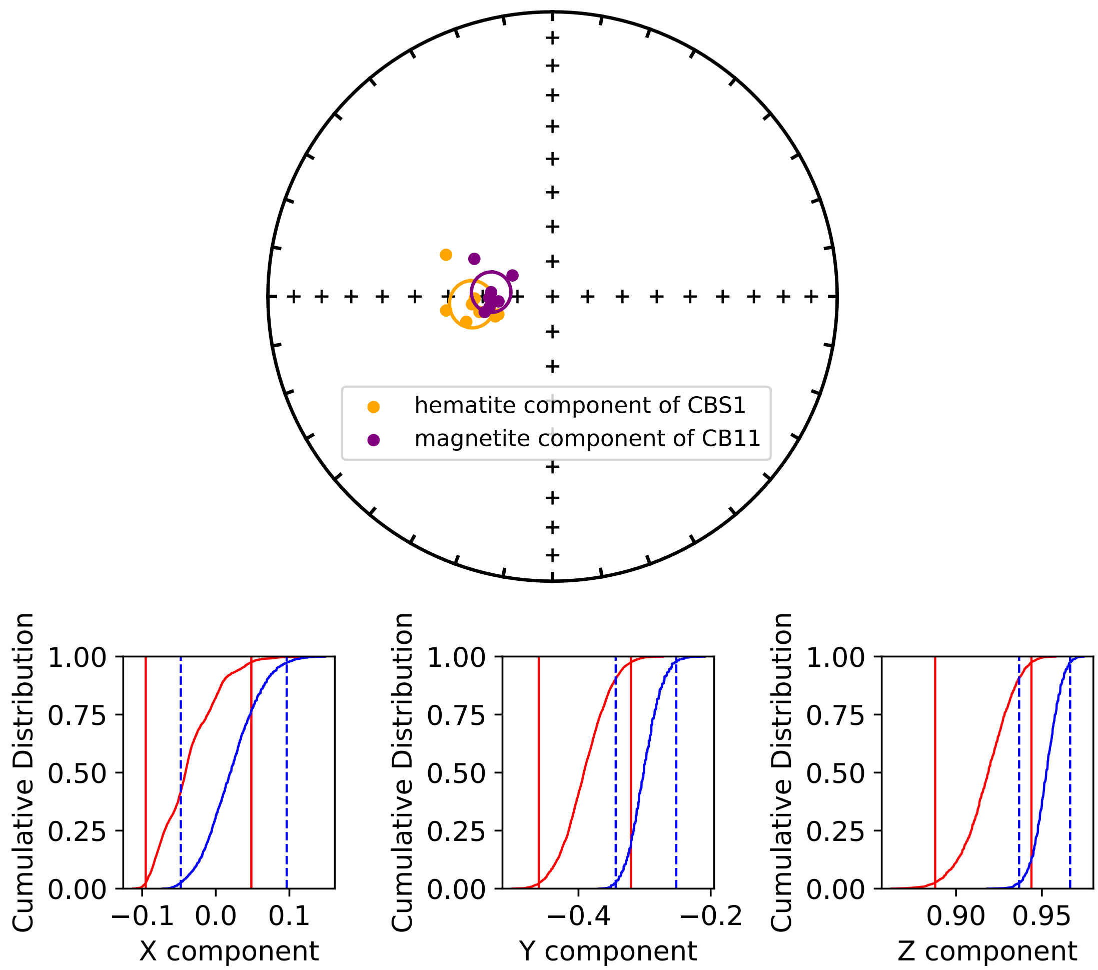

Figure S3. Top: Equal area plot showing the hematite magnetization specimen directions (orange) of the interflow sandstone CBS1 which is stratigraphically below the CB11 lava flow, whose magnetite magnetization directions are shown in purple. Bottom: Bootstrap common mean test of Tauxe et al. (1991) between the specimens directions of the sandstone and the lava flow show a positive result. The specimen directions also passes a common mean test of McFadden and McElhinny (1990) with a 'B' classification and have a positive support for sharing a common mean based on the Bayesian approach of Heslop et al. (2023).

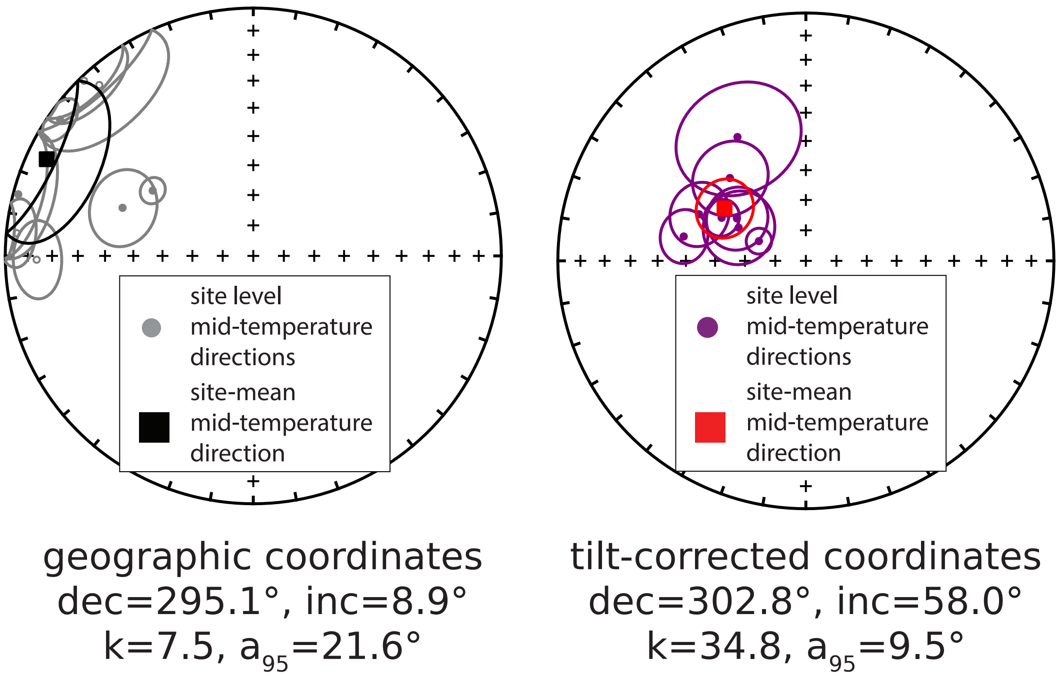

Figure S4. Equal area plots showing the site-level directions and site-mean directions of the Death Valley diabase sills that yielded coherent within-site thermal demagnetization results in both geographic coordinates (left) and tilt-corrected coordinates (right). The site-mean direction in geographic coordinates is dec=295.1°, inc=8.9°, n=8, k=7.5, a_{95}=21.6°. The site-mean direction in tilt-corrected coordinates is dec=302.8°, inc=58.0°, k=34.8, a_{95}=9.5°. Applying tilt correction to the sills significantly improves the grouping of the site level directions.

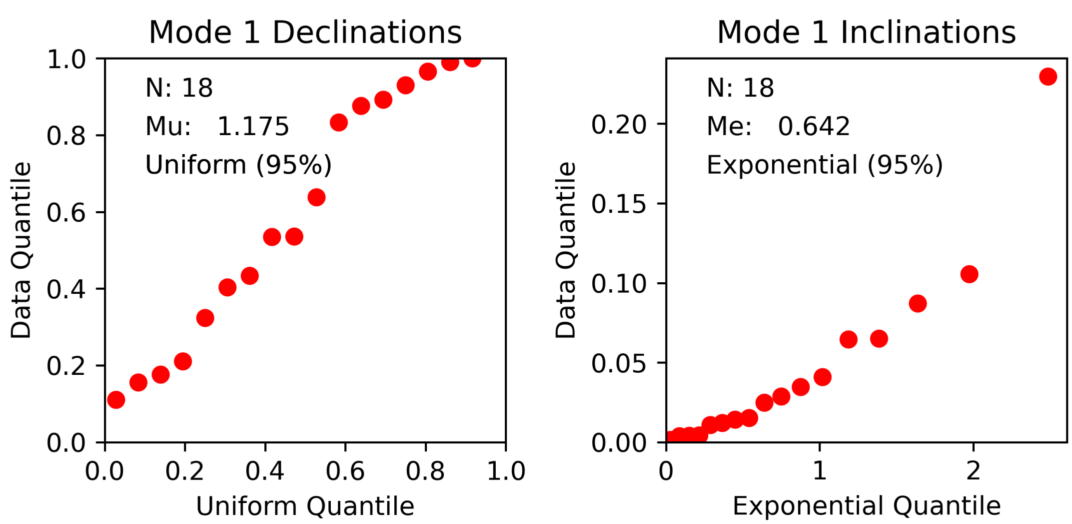

Figure S5. Fisher quantile-quantile Fisher et al. (1987) test of the distribution of the site level virtual geomagnetic poles of the Cardenas Basalt lava flows. The results show that the null hypothesis that the VGPs are Fisher-distributed cannot be rejected.

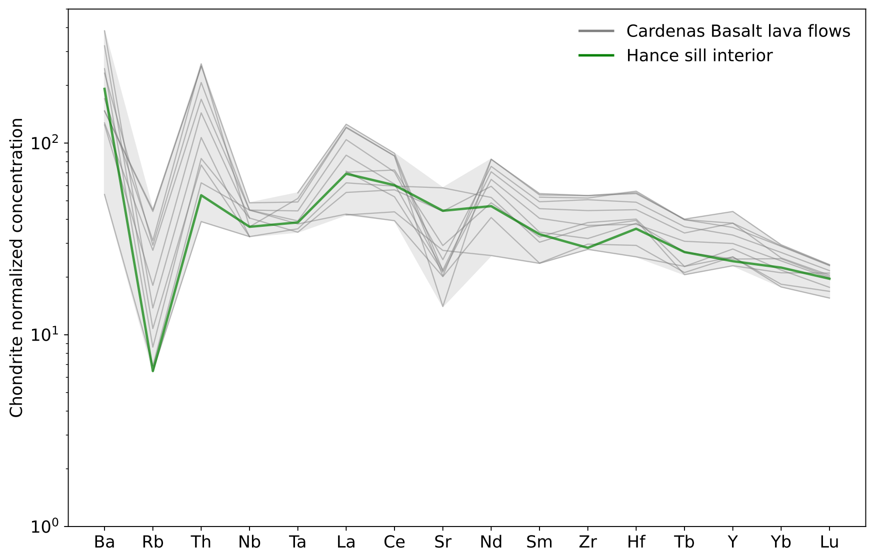

Figure S6. Trace element geochemistry data from Larson et al. (1994). The elemental abundance of the interior of the Hance sill is similar to that of the Cardenas Basalt lavas. Virtual geomagnetic poles developed from the Hance sill, Hance dike, and another undated sill in Red Canyon adjacent to Hance rapids plot closer to those of the Cardenas Basalt than the dated ca. 1098 Ma poles as shown in the main text. These data are consistent with the interpretation that the intrusions near Hance rapids are feeders to the Cardenas Basalt.

References

Donadini, F., Pesonen, L. J., Korhonen, K., Deutsch, A., and Harlan, S. S., 2011, Paleomagnetism and paleointensity of the 1.1 Ga old diabase sheets from central Arizona: Geophysica, vol. 47, pp. 3–30.

Driscoll, P. E. and Evans, D. A., 2016, Frequency of Proterozoic geomagnetic superchrons: Earth and Planetary Science Letters, vol. 437, pp. 9–14, doi:10.1016/j.epsl.2015.12.035.

Fisher, N. I., Lewis, T., and Embleton, B. J., 1987, Statistical analysis of spherical data: Cambridge university press.

Haggerty, S. E. and Baker, I., 1967, The alteration of olivine in basaltic and associated lavas: Contributions to Mineralogy and Petrology, vol. 16, pp. 233–257, doi:10.1007/bf00371094.

Harlan, S. S., 1993, Paleomagnetism of Middle Proterozoic diabase sheets from central Arizona: Canadian Journal of Earth Sciences, vol. 30, pp. 1415–1426, doi:10.1139/e93-122.

Hedley, I., 1968, Chemical remanent magnetization of the FeOOH, Fe2O3 system: Physics of the Earth and Planetary Interiors, vol. 1, pp. 103–121, doi:10.1016/0031-9201(68)90055-1.

Hendricks, J. D., 1989, Petrology and chemistry of igneous rocks of Middle Proterozoic Unkar Group, Grand Canyon Supergroup, northern Arizona: *In* Geology of Grand Canyon, Northern Arizona (with Colorado River Guides): Lee Ferry to Pierce Ferry, Arizona, American Geophysical Union, pp. 106–116, doi:10.1029/ft115p0106.

Heslop, D., Scealy, J. L., Wood, A. T. A., Tauxe, L., and Roberts, A. P., 2023, A bootstrap common mean direction test: Journal of Geophysical Research: Solid Earth, vol. 128, doi:10.1029/2023jb026983.

Larson, E., Patterson, P., and Mutschler, F., 1994, Lithology, chemistry, age, and origin of the Proterozoic Cardenas Basalt, Grand Canyon, Arizona: Precambrian Research, vol. 65, pp. 255–276, doi:10.1016/0301-9268(94)90108-2.

McClelland, E., 1987, Self-reversal of chemical remanent magnetization: a palaeomagnetic example: Geophysical Journal International, vol. 90, pp. 615–625, doi:10.1111/j.1365-246x.1987.tb00744.x.

Mcclelland, E. and Goss, C., 1993, Self reversal of chemical remanent magnetization on the transformation of maghemite to haematite: Geophysical Journal International, vol. 112, pp. 517–532, doi:10.1111/j.1365-246x.1993.tb01185.x.

McFadden, P. and McElhinny, M., 1990, Classification of the reversal test in palaeomagnetism: Geophysical Journal International, vol. 103, pp. 725–729, doi:10.1111/j.1365-246X.1990.tb05683.x.

Swanson-Hysell, N. L., Feinberg, J. M., Berquó, T. S., and Maloof, A. C., 2011, Self-reversed magnetization held by martite in basalt flows from the 1.1-billion-year-old Keweenawan rift, Canada: Earth and Planetary Science Letters, vol. 305, pp. 171–184, doi:10.1016/j.epsl.2011.02.053.

Swanson-Hysell, N. L., Ramezani, J., Fairchild, L. M., and Rose, I. R., 2019, Failed rifting and fast drifting: Midcontinent Rift development, Laurentia's rapid motion and the driver of Grenvillian orogenesis: GSA Bulletin, vol. 131, pp. 913–940, doi:10.1130/b31944.1.

Tauxe, L., Kylstra, N., and Constable, C., 1991, Bootstrap statistics for paleomagnetic data: Journal of Geophysical Research, vol. 96, p. 11,723, doi:10.1029/91jb00572.